ELSEVIER

Biochimica et Biophysica Acta 1194 (1994) 99–108

BBA Biochimica et Biophysica Acta

Properties of phosphatidylcholine bilayers as revealed by mixed-acyl phospholipid fluorescent probes containing *n*-(9-anthroyloxy) fatty acids

Jeffrey T. Mason *

Department of Cellular Pathology, Armed Forces Institute of Pathology, Washington, DC 20306-6000, USA

Received 9 March 1994

Abstract

A series of five mixed-acyl phosphatidylcholine (PC) fluorescent probes having the structure 1-caproyl-2-(*n*-(9-anthroyloxy)-acyl)-*sn*-glycero-3-phosphocholine, where the *sn*-2 anthroyloxy-labeled acyl chain is stearic acid ($n = 2,6,9,12$) or palmitic acid ($n = 16$), have been prepared. These probes have been used to study the thermal behavior and transbilayer organization of 1,2-distearoyl-PC (C(18)C(18)PC), 1-stearoyl-2-caproyl-PC (C(18)C(10)PC), and 1-caproyl-2-stearoyl-PC (C(10)C(18)PC) multilamellar dispersions. These probes reported the noninterdigitated gel to liquid-crystalline phase transition of C(18)C(18)PC at 55.1°C and the mixed-interdigitated gel to liquid-crystalline phase transitions of C(18)C(10)PC and C(10)C(18)PC at 19.1 and 10.1°C, respectively. The results suggest that, upon cooling, the C(18)C(10)PC liquid-crystalline phase transforms to the mixed-interdigitated gel phase by way of a partially interdigitated gel-phase intermediate. Isothermal plots of anisotropy versus the position of the anthroyl moiety on the *sn*-2 acyl chain of the PC probes were used to construct transbilayer anisotropy profiles of the gel phases of the three bilayer systems. These anisotropy profiles can serve as 'interdigitation signatures' that clearly distinguish the noninterdigitated from the mixed-interdigitated gel-phase bilayer organization. In the liquid-crystalline phase, the anisotropy profiles suggest that the dynamic motions of the disordered acyl chains of the mixed-acyl PCs are influenced by the interpenetration of the chains from the opposing leaflets of the bilayer.

Key words: Phospholipid bilayer; Bilayer interdigitation; Fluorescent probe; Anthroyloxy fatty acid; Fluorescence emission anisotropy

1. Introduction

X-ray diffraction studies by Hui et al. [1] and McIntosh et al. [2] have demonstrated that hydrated bilayers composed of 1-stearoyl-2-caproyl-*sn*-glycero-3-phosphocholine (C(18)C(10)PC) adopt a gel-phase organization such that the short caproyl chains pack end-to-end and the long stearoyl chains span the entire width of the hydrocarbon core of the bilayer. This has been termed a mixed-interdigitated bilayer packing [1]. Subsequent studies [3,4] have shown this gel-phase packing to be characteristic of mixed-chain PCs and phosphatidylethanolamines whose long hydrocarbon chains are twice the length of their short chains. In addition to synthetic phospholipids, mixed-interdigitated packings have been proposed for bilayers consisting of naturally occurring glycosphingolipids, sphingomyelins [5], and sulfatides [6]. Consequently, the mixed-interdigitated bilayer packing could be relevant to the normal or pathologic organization of biomembranes. To date, X-ray diffraction [1,2] and electron spin resonance [7] have been the only reliable techniques for identifying the presence of interdigitated packings in

Abbreviations: PC, phosphatidylcholine; C(x)C(y)PC, a saturated phosphatidylcholine with x carbons in the *sn*-1 acyl chain and y carbons in the *sn*-2 acyl chain; DSC, differential scanning calorimetry; *n*-AS(AP)-PC, a 1-caproyl-2-(*n*-(9-anthroyloxy)acyl)-*sn*-glycero-3-phosphocholine where n is the site of attachment of the fluorophore on the *sn*-2 acyl chain, AS = *n*-(9-anthroyloxy)stearic acid, and AP = *n*-(9-anthroyloxy)palmitic acid; T_m, phase transition temperature (in °C) as measured by DSC; T_f, phase transition temperature (in °C) as measured by fluorescence spectroscopy (T_f^a for ascending temperature scans and T_f^d for descending temperature scans); T_o and T_c, phase transition onset and completion temperatures (in °C), respectively, as measured by fluorescence spectroscopy; $\Delta T_{1/2}$, phase transition width (in °C) at half-maximal excess heat capacity as measured by DSC; ΔH, phase transition enthalpy change (in kcal/mol) as measured by DSC.

* Corresponding author. Fax: +1 (202) 5762164.

SSDI 0005-2736(94)00127-B

bilayer assemblies. However, due to the limited availability of these instruments, alternative techniques for detecting the mixed-interdigitated bilayer organization would be useful.

The principal distinguishing feature of the mixed-interdigitated packing is the transbilayer organization exhibited by the phospholipid hydrocarbon chains. Thus, a technique that is sensitive to this transbilayer organization should be able to distinguish between the mixed-interdigitated and the normal noninterdigitated chain packings. Previous studies have shown that a series of *n*-(9-anthroyloxy) fatty acids ($n = 2,6,9,12,16$) fit in the bilayer with their acyl chains parallel to those of the phospholipids. The fluorophores of these probes locate at a graded series of depths in the bilayer as demonstrated by energy transfer [8], NMR [9], and fluorescence quenching [10] studies. These fluorescent probes have been used to assess the anisotropy gradients in bilayers composed of symmetric-chain phospholipids [11] and have yielded anisotropy profiles similar to the order-parameter profiles obtained by NMR [12] and electron spin resonance [13] spectroscopy.

Five mixed-acyl PC fluorescent probes with the structure 1-caproyl-2-(*n*-(9-anthroyloxy)acyl)-*sn*-glycero-3-phosphocholine, where the *sn*-2 anthroyloxy-labeled acyl chain is stearic acid ($n = 2,6,9,12$) or palmitic acid ($n = 16$), have been prepared and studied. These probes, which are referred to as 2-AS-PC, 6-AS-PC, 9-AS-PC, 12-AS-PC, and 16-AP-PC, respectively, have been used to determine the anisotropy profiles in noninterdigitated (C(18)C(18)PC) and mixed-interdigitated (C(18)C(10)PC and C(10)C(18)PC) bilayers. The results indicate that the anisotropy profiles can distinguish between the two different gel-phase bilayer packings. In the liquid-crystalline phase, the anisotropy profiles suggest that the dynamic motions of the disordered acyl chains of the mixed-acyl PCs are influenced by the interpenetration of chains from opposing leaflets of the bilayer. In addition, the findings provide an explanation for the hysteresis seen by differential scanning calorimetry (DSC) in the gel ↔ liquid-crystalline phase transition of C(18)C(10)PC dispersions.

2. Materials and methods

2.1. Materials

Synthetic C(18)C(18)PC and C(10)C(10)PC were purchased from Avanti Polar Lipids. (Alabaster, AL) and were checked for purity by thin-layer chromatography on 250-μm silica gel G plates by using a solvent system of chloroform/methanol/48% ammonium hydroxide (65:35:5, v/v) followed by visualization with iodine. In both cases, only a single spot, corresponding to authentic PC, was observed at a loading of 1 μmol of lipid. A set of *n*-(9-anthroyloxy)stearic acids ($n = 2,6,9,12$) and 16-(9-anthroyloxy)palmitic acid were purchased from Molecular Probes (Eugene, OR). Their purity was confirmed by thin-layer chromatography employing ethanol/water (95:5, v/v) as solvent followed by visualization with iodine [14]. Doubly distilled water was used for the preparation of all buffer solutions. All other reagents were of the highest grade commercially available.

2.2. Phospholipid synthesis

The five mixed-acyl PC fluorescent probes were synthesized by a modification of the method of Mason et al. [15]. Briefly, C(10)C(10)PC was subjected to enzymatic hydrolysis with phospholipase A_2, and the resulting 1-caproyl-lysoPC was purified by precipitation from ether. The lysoPC was then reacylated by employing the anhydride of one of the *n*-(9-anthroyloxy) fatty acids. The anhydrides were prepared by the method of Selinger and Lapidot [16]. The reacylation reaction was performed in dry, ethanol-free chloroform at room temperature employing a 2-fold excess of anhydride and a 2.5-fold excess of 4-pyrrolidinopyridine as catalyst. The resulting mixed-acyl PC was purified by elution from silicic acid employing a gradient of methanol in chloroform. During the synthesis, the reaction intermediates were shielded from light as much as possible, and all solvents were deoxygenated with argon prior to use. A total of five mixed-acyl PC fluorescent probes were prepared corresponding to the five carbon esterification sites (2,6,9,12,16) of the anthroyl moiety on the *sn*-2 acyl chain. The purity of the PCs was confirmed by thin-layer chromatography as described above. Finally, the PC probes were precipitated three times from acetone/chloroform (95:5, v/v), dried, and stored desiccated at −20°C. The C(18)C(10)PC and C(10)C(18)PC employed in the study were prepared in an analogous manner.

2.3. Preparation of samples for DSC and fluorescence spectroscopy

C(18)C(18)PC, C(18)C(10)PC, or C(10)C(18)PC was combined with one of the mixed-acyl PC fluorescent probes at a probe to PC molar ratio of 1:500. Ratios varying from 1:100 to 1:700 were examined and found to have no effect on the DSC or fluorescence anisotropy results. The lipid mixture was dissolved in spectral benzene/methanol (95:5, v/v), frozen, and lyophilized for 12 h. The dried lipid mixture was dispersed in buffer at 60°C (C(18)C(18)PC) or 30°C (C(18)C(10)PC and C(10)C(18)PC) and vortexed. The preparation was

then cycled five times between 0 and 60°C (C(18)C(18) PC) or 0 and 30°C (C(18)C(10)PC and C(10)C(18)PC) with occasional vortexing. This protocol resulted in the production of large multilamellar vesicles that lack any radius-of-curvature effects. Thus, since the fluorescent probes were present in the dry films when they were hydrated, it can be assumed that the probes were symmetrically incorporated into both leaflets of the phospholipid bilayers. Buffers employed were 50 mM KCl for DSC and 50 mM KCl containing 15% (w/v) sucrose for fluorescence. The sucrose prevented precipitation of the liposomal dispersions during fluorescence measurements and had no effect on the measured anisotropy values. Total PC concentrations employed were 20 mg/ml for DSC and 0.1 mM for fluorescence. PC concentrations were determined by the method of inorganic phosphate [17]. C(18)C(18)PC and C(18)C(10)PC samples were allowed to anneal at 5°C for 1 week prior to analysis by DSC or fluorescence spectroscopy. C(10)C(18)PC samples were incubated at 5°C for only 12 h because prolonged incubation at low temperatures will convert the metastable mixed-interdigitated gel phase of this PC to a stable partially interdigitated crystalline phase [18]. During the preparation steps, the lipids were shielded from light as much as possible.

2.4. DSC

All DSC runs were performed on a Hart 7707 series differential scanning microcalorimeter (Hart Scientific, Provo, UT) as described [4]. Samples (~500 μl of solution) were loaded into 1-ml stainless steel vials, which were sealed and incubated in the calorimeter at the desired starting temperature. The solutions were allowed to come to thermal equilibrium, which typically required 1 h, prior to the initiation of the run. Scans were performed in both the ascending and descending temperature direction at a scan rate of 10°C/h. After baseline subtraction and correction for the instrument thermal response, the calorimetric data were analyzed to yield phospholipid excess heat capacities as a function of temperature and enthalpy changes (ΔH) by using software supplied by Hart. For a given phase transition, the transition temperature (T_m) was taken to be the temperature of the maximal excess heat capacity, and $\Delta T_{1/2}$ was taken as the transition width at half-maximal excess heat capacity.

2.5. Fluorescence measurements

Steady-state fluorescence emission anisotropies were measured with a Perkin-Elmer MPF3 spectrofluorometer (Perkin-Elmer, Norwalk, CT) equipped with a xenon light source, a thermostated cell holder, and rotatable polarizers (Polarex; E. Kasemann Optische, Germany). Fluorescence emission was detected at a 90° angle from the excitation beam. An excitation wavelength of 385 nm, with bandwidths of 2–5 nm, was employed. Fluorescence emission was detected at a wavelength of 450 nm with bandwidths of 12–16 nm. A 430-nm emission cutoff filter was used, and the instrument gain was set to 100. Relative intensities were recorded in the ratio mode to eliminate the effect of source intensity fluctuations. The PC dispersions (3 ml) were loaded into quartz cuvettes and placed in the thermostated cell holder. The temperature of the cell holder was controlled with a programmable water bath that was set to scan in the ascending or descending temperature direction at 10°C/h. Sample temperature was monitored with a YSI thermistor (YSI, Yellow Springs, OH) inserted directly into the cuvette but above the light path. During the scans, the intensities of the parallel ($I_{\parallel}$) and perpendicular ($I_{\perp}$) components of the emitted light, as well as sample temperature, were recorded at intervals of ~0.5°C. The contribution of scattered light to the fluorescence emission ($I_{\parallel}^{s}$ and $I_{\perp}^{s}$) was determined independently for an unlabeled reference solution of the same composition. At the PC concentrations employed, the contribution of scattered light to the total fluorescence emission was less than 2%. The steady-state fluorescence emission anisotropy was calculated as

$$r = \frac{(I_{\parallel} - I_{\parallel}^{s}) - G(I_{\perp} - I_{\perp}^{s})}{(I_{\parallel} - I_{\parallel}^{s}) + 2G(I_{\perp} - I_{\perp}^{s})}$$

where r is the anisotropy and G is the instrument grating correction factor. This factor was determined by measuring the depolarization of *N*-methylacridinium perchlorate in methanol (excitation 360 nm, emission 430 nm), which is completely depolarized at room temperature.

3. Results

3.1. Anisotropy–temperature plots

The five mixed-acyl PC fluorescent probes were incorporated, individually, into C(18)C(18)PC, C(18)C(10)PC, and C(10)C(18)PC bilayers, and the anisotropy of the probes as a function of temperature was determined. Ascending and descending temperature scans were performed from 30 to 75°C (C(18)C(18)PC) or from 2 to 30°C (C(18)C(10)PC and C(10)C(18)PC).

Representative ascending temperature plots are shown in Fig. 1 for C(18)C(18)PC bilayers containing the probes 6-AS-PC (Fig. 1A) and 16-AP-PC (Fig. 1B).

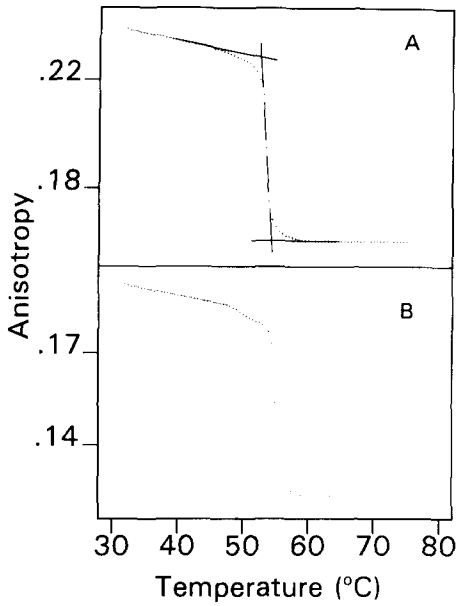

Fig. 1. Anisotropy versus ascending temperature plots for C(18)C(18)PC bilayers containing the probes 6-AS-PC (A) and 16-AP-PC (B). The projected lines in panel A demonstrate the determination of the onset (T_o) and completion (T_c) temperatures of the thermal phase transitions.

Table 1
Fluorescence parameters of the five mixed-acyl PC fluorescent probes in symmetric-chain and mixed-acyl phospholipid bilayers

Bilayer	Probe	T_f^a (°C)	T_f^d (°C)	$T_f^a - T_f^d$ (°C)
C(18)C(18)PC	2-AS-PC	52.9	52.5	0.4
	6-AS-PC	53.5	53.0	0.5
	9-AS-PC	54.2	53.7	0.5
	12-AS-PC	54.5	53.6	0.9
	16-AP-PC	55.1	54.6	0.5
C(18)C(10)PC	2-AS-PC	16.9	16.6	0.3
	6-AS-PC	19.1	17.6	1.5
	9-AS-PC	19.1	15.0	4.1
	12-AS-PC	16.9	14.6	2.3
	16-AP-PC	18.9	15.2	3.7
C(10)C(18)PC	2-AS-PC	9.3	9.1	0.2
	6-AS-PC	10.5	9.9	0.6
	9-AS-PC	10.3	9.8	0.5
	12-AS-PC	9.4	9.1	0.3
	16-AP-PC	9.4	9.4	0.0

The five mixed-acyl PC fluorescent probes were incorporated, individually, into C(18)C(18)PC, C(18)C(10)PC, and C(10)C(18)PC bilayer dispersions, and their plots of steady-state emission anisotropy as a function of temperature were determined. An excitation wavelength of 385 nm was employed. The associated fluorescence parameters were determined from these plots.

The excitation wavelength used for these measurements was 385 nm. The anisotropy versus temperature plots for C(18)C(18)PC bilayers containing the other three fluorescent PC probes were similar to those of Fig. 1. The plots of anisotropy versus temperature clearly delineate the gel ↔ liquid-crystalline phase transition at 55°C. Also, the pretransition at 52°C is evident as a modest curvilinear depression of the anisotropy immediately preceding the main thermal phase transition. The corresponding descending temperature plots (not shown) were almost identical except for a small hysteresis and the absence of the pretransition. Despite the pretransition, it is possible to divide the anisotropy plots into three roughly linear regions corresponding to the gel phase, the liquid-crystalline phase, and the phase transition region (Fig. 1A). The intersection of these linear projections was used to define the phase transition onset (T_o) and completion (T_c) temperatures and the phase transition temperature (T_f), which was calculated as $(T_o + T_c)/2$. Transition temperatures were calculated from both ascending (T_f^a) and descending (T_f^d) temperature plots. These parameters are listed in Table 1 for the five mixed-acyl PC fluorescent probes. The value of T_m (the phase transition temperature measured by DSC) and T_f^a were equal for 16-AP-PC in C(18)C(18)PC bilayers, but the remaining T_f^a values decreased as the fluorophore was moved toward the glycerol region.

Fig. 2 shows representative anisotropy versus temperature plots (both ascending and descending temperature) for C(18)C(10)PC bilayers containing the probes 6-AS-PC (Fig. 2A) and 16-AP-PC (Fig. 2B). The anisotropy versus temperature plots for C(18)C(10)PC bilayers containing the other three fluorescent probes were similar to those of Fig. 2. Both of these probes delineate the mixed-interdigitated gel ↔ liquid-crystalline phase transition at 19°C that is characteristic of C(18)C(10)PC bilayers. The hysteresis (T_f^a–T_f^d) mea-

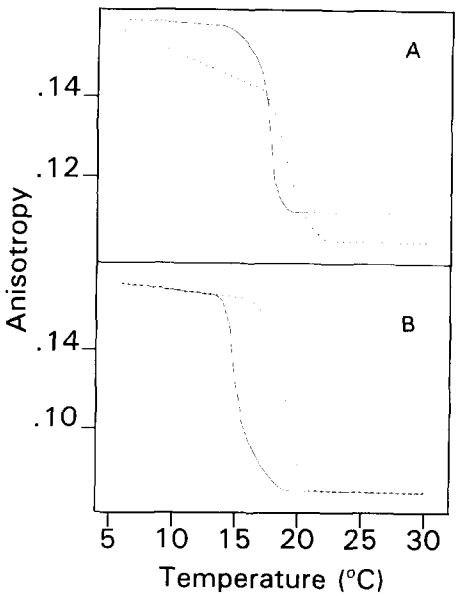

Fig. 2. Anisotropy versus temperature plots for C(18)C(10)PC bilayers containing the probes 6-AS-PC (A) and 16-AP-PC (B). Both ascending (+ + +) and descending (———) temperature scans are shown.

sured for the phase transition was sensitive to the position of the fluorophore on the mixed-acyl PC probe. The hysteresis was small for the probes 2-AS-PC and 6-AS-PC, with values of 0.3 and 1.5°C, respectively. In contrast, the hysteresis was much larger for the probes 9-AS-PC, 12-AS-PC, and 16-AP-PC, with values of 4.1, 2.3, and 3.7°C, respectively. There was a hysteresis in the anisotropy values in the liquid-crystalline phase for the probes 6-AS-PC and 9-AS-PC; it was about 0.008 units lower for the ascending temperature scans. This hysteresis was observed whenever the preparations were incubated in the liquid-crystalline phase for several hours prior to the initiation of the descending temperature scan. The source of this hysteresis is not known.

Plots of anisotropy versus temperature were measured for C(10)C(18)PC bilayers containing the five mixed-acyl PC fluorescent probes (not shown). The fluorescence parameters determined from these plots are listed in Table 1. The values of $T_f^a - T_f^d$ for the C(10)C(18)PC bilayers did not exhibit the irregular behavior seen with C(18)C(10)PC. Instead, the hysteresis in the phase transition temperatures averaged less than 1°C and was independent of fluorophore position. Otherwise, the anisotropy versus temperature plots for the C(10)C(18)PC bilayers were similar to those measured for C(18)C(10)PC.

3.2. DSC of fluorophore-containing mixed-acyl PC bilayers

DSC measurements were performed on C(18)C(10) PC bilayers containing the mixed-acyl PC fluorescent probes at the same probe to PC molar ratio (1:500) used for the fluorescence measurements. Ascending and descending temperature scans were performed from 5 to 35°C. Representative DSC profiles are shown in Fig. 3 for C(18)C(10)PC bilayers containing the probes 6-AS-PC (Fig. 3A and B) and 16-AP-PC (Fig. 3C and D). Both ascending temperature scans displayed single endothermic transitions that yielded values of $T_m = 19.1$°C, $\Delta T_{1/2} = 0.61$°C, and $\Delta H = 9.1$ kcal/mol. The descending temperature scans each displayed two partially resolved exotherms. The higher temperature exotherms (transition temperature T_m^H) yielded values of $T_m^H = 17.7$°C, $\Delta T_{1/2} = 0.37$°C, and $\Delta H = 1.06$ kcal/mol. The lower temperature exotherms (transition temperature T_m^L) yielded values of $T_m^L = 14.6$°C, $\Delta T_{1/2} = 0.79$°C, and $\Delta H = 6.9$ kcal/mol. These thermodynamic parameters are identical to those exhibited by pure C(18)C(10)PC dispersions [19]. Analogous results were obtained for C(18)C(10)PC bilayers containing the other three mixed-acyl PC fluorescent probes.

DSC measurements were also performed on C(10) C(18)PC bilayers containing the five mixed-acyl PC fluorescent probes (not shown). Again, the thermodynamic parameters for these preparations were identical to those exhibited by pure C(10)C(18)PC dispersions [19]. Ascending temperature scans revealed a single endothermic phase transition with values of $T_m = 10.1$°C, $\Delta T_{1/2} = 0.95$°C, and $\Delta H = 5.7$ kcal/mol. Descending temperature scans also revealed a single exothermic phase transition with values of $T_m = 9.8$°C, $\Delta T_{1/2} = 0.88$°C, and $\Delta H = 5.8$ kcal/mol.

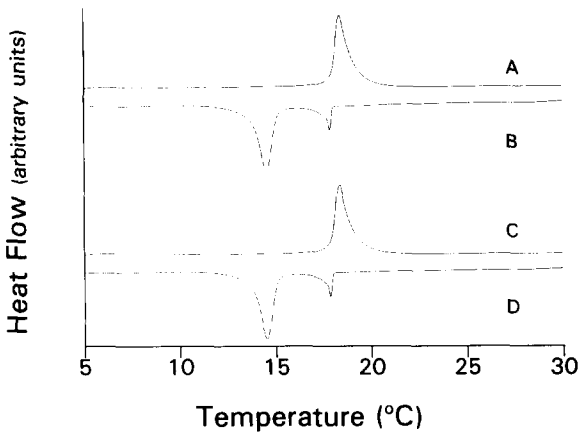

Fig. 3. DSC heating (A and C) and cooling (B and D) thermograms of C(18)C(10)PC bilayers containing the probes 6-AS-PC (A and B) and 16-AP-PC (C and D). The probe to PC molar ratios were 1:500.

3.3. Anisotropy–position plots

Isothermal plots of anisotropy versus the position of the *n*-(9-anthroyloxy) fluorophore on the *sn*-2 acyl chain of the PC probes were determined at temperatures within the gel and liquid-crystalline phase regions of the C(18)C(18)PC, C(18)C(10)PC, and C(10)C(18)PC bilayers. These isothermal plots were determined from plots of anisotropy versus temperature like those in Figs. 1 and 2. The plots of anisotropy versus fluorophore position for C(18)C(18)PC bilayers in the gel (45°C) and liquid-crystalline (65°C) phases are shown in Fig. 4A. In the gel phase, there is a slow linear decrease in anisotropy as the fluorophore is moved from position 2 to 12, after which the anisotropy drops slightly at the bilayer center. In the liquid-crystalline phase, there is a linear decrease in anisotropy between positions 2 and 16, with the gradient being steeper than that between positions 2 and 12 in the gel phase. The plots of anisotropy versus fluorophore position for C(18)C(10)PC bilayers in the gel (8°C) and liquid-crystalline (30°C) phases are shown in Fig. 4B. In the gel phase, the anisotropy decreases between positions 2 and 6, increases between positions 6 and 9, and then decreases slowly through the end of the chain. In the liquid-crystalline phase, the profile is similar, but the overall anisotropy values are lower. In addition, there is a smaller increase in anisotropy between positions 6 and 9 and a larger decrease between positions 12 and

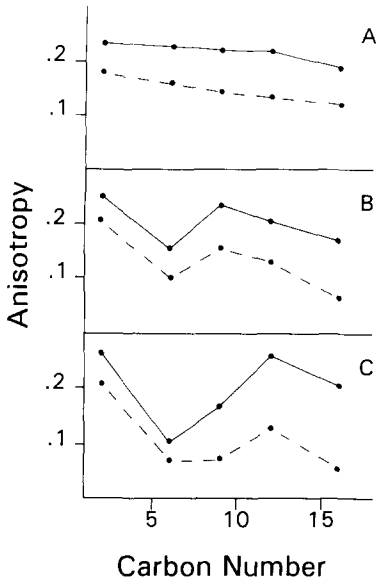

Fig. 4. Isothermal plots of anisotropy versus the position of the *n*-(9-anthroyloxy) fluorophore on the *sn*-2 acyl chain of the PC probes in the gel (———) and liquid-crystalline (— — —) phase regions of C(18)C(18)PC (A; 45°C gel, 65°C liquid-crystalline), C(18)C(10)PC (B; 8°C gel, 30°C liquid-crystalline), and C(10)PC(18)PC (C; 2°C gel, 20°C liquid-crystalline) bilayer dispersions.

16 than those observed in the gel-phase profile. Isothermal plots of anisotropy versus fluorophore position for C(10)C(18)PC bilayers in the gel (2°C) and liquid-crystalline (20°C) phases are shown in Fig. 4C. Overall, these profiles are similar to those obtained with C(18)C(10)PC, but the exact patterns differ slightly.

4. Discussion

4.1. Anisotropy–temperature plots

In this study a series of five anthroyloxy-labeled mixed-acyl PC fluorescent probes were prepared. These probes were used to study the thermal behavior and transbilayer organization of C(18)C(18)PC, C(18)C(10)PC, and C(10)C(18)PC multilamellar dispersions. When incorporated into C(18)C(18)PC bilayers, these probes reported the main gel ↔ liquid-crystalline phase transition at 55°C. These probes were also sensitive to the $L_{\beta'} \leftrightarrow P_{\beta'}$ pretransition at 52°C: the sensitivity increased as the fluorophore was moved deeper into the bilayer. The value of T_f^a decreased as the fluorophore was moved from the chain terminus (16-AP-PC) to the polar interface (2-AS-PC). This pattern is believed to be a relative measure of the fluorophore's perturbation of its local environment; it is least perturbed at the bilayer center [20]. The behavior of these probes is identical to that of *n*-(9-anthroyloxy) fatty acids incorporated into C(16)C(16)PC bilayers [20–24]. Thus, the fluorophore of the mixed-acyl PC fluorescent probes is sensitive to the local environment of the C(18)C(18)PC bilayer despite being covalently attached to a mixed-acyl PC host.

When incorporated into C(18)C(10)PC and C(10)C(18)PC bilayers, the five mixed-acyl PC fluorescent probes sensed the mixed-interdigitated gel to liquid-crystalline phase transition that occurs in these bilayers at 19.1°C and 10.1°C, respectively. During descending temperature fluorescence scans of the C(18)C(10)PC bilayers, the thermotropic behavior as reflected by the probes was sensitive to the position of the anthroyl moiety on the acyl chain (Fig. 2). The probes 2-AS-PC and 6-AS-PC appear to reflect the high-temperature transition (T_m^H), whereas the probes 9-AS-PC, 12-AS-PC, and 16-AP-PC appear to reflect the low-temperature transition (T_m^L) identified by DSC during descending temperature scans of this PC. The DSC profiles indicated that this behavior does not arise from a perturbation of the bulk lipid properties by the fluorescent probes. The following hypothesis is consistent with these observations. When cooled, the C(18)C(10)PC bilayer undergoes a transition from the liquid-crystalline phase to a partially interdigitated gel phase at T_m^H. In the partially interdigitated bilayer, the long chains of the PCs in one bilayer leaflet pack end-to-end with the short chains from PCs in the opposing bilayer leaflet. This is analogous to the gel-phase packing adopted by C(18)C(14)PC bilayers [25]. Raman spectroscopic [26] and X-ray diffraction [1] studies have shown that the liquid-crystalline to partially interdigitated gel-phase transition of C(18)C(14)PC results in the ordering of both lipid acyl chains down to the level of the short myristoyl chain. The terminal segments of the stearoyl chains, below the level of the myristoyl chains, remain disordered. By analogy, the liquid-crystalline to partially interdigitated gel-phase transition of C(18)C(10)PC would involve an ordering of the upper chain segments, down to the level of the caproyl chains, as reflected by the probes 2-AS-PC and 6-AS-PC. At T_m^L the partially interdigitated gel phase transforms to the mixed-interdigitated gel phase. This phase transition would result in the ordering of the terminal segments of the stearoyl chains as a consequence of the adoption of the mixed-interdigitated chain packing, while the upper lipid acyl chain segments remain ordered. Thus, the partially interdigitated to mixed-interdigitated gel-phase transition would be reflected, principally, by the probes 9-AS-PC, 12-AS-PC, and 16-AP-PC. In contrast, descending temperature scans of C(10)C(18)PC bilayers obtained by DSC revealed a single liquid-crystalline ↔ mixed-interdigitated gel phase transition at 9.8°C. Accordingly, no biphasic behavior of the T_f^d values for C(10)C(18)PC were observed, and the corresponding $T_f^a - T_f^d$ values were all less than 1°C.

4.2. Anisotropy-position plots

The use of *n*-(9-anthroyloxy) fatty acids to assess anisotropy gradients in phospholipid bilayers is predicated on the assumption that the location of the fluorophore in the bilayer is accurately known. As stated previously, numerous studies [8–10] have shown that the *n*-(9-anthroyloxy) fatty acids fit into the bilayer with their acyl chains oriented parallel to those of the phospholipids and with their anthroyl moieties located at a graded series of depths in the bilayer. It is reasonable to assume that the *n*-(9-anthroyloxy) fatty acids used in this study behave in an analogous manner by virtue of their covalent attachment to a mixed-acyl PC host.

The fluorescence emission anisotropy of the anthroyloxy PC probes is a function of both the resistance to depolarizing rotations and the orientational constraint imposed by the anisotropic phospholipid environment [28]. In addition, the motion of the aromatic anthroyl ring is the result of at least two principal modes of rotation [29]. The out-of-plane rotational mode results from rotation of the anthroyl ring around its ester linkage and is observed at an excitation wavelength of 316 nm. The in-plane rotational mode is dependent upon reorientation of the acyl chain to which the fluorophore is attached. The fluorescence emission anisotropy reflects both modes of motion at an excitation wavelength of 385 nm. The interpretation of the steady-state fluorescence emission anisotropy is further complicated by hindered rotational motions of the fluorescent probes. Time-resolved emission anisotropy measurements by Vincent et al. [29] have shown that the out-of-plane mode of rotation is unhindered in both the gel and liquid-crystalline phases of C(16)C(16)PC bilayers, whereas the in-plane mode of rotation is only unhindered above the gel ↔ liquid-crystalline transition. Studies by Thulborn and Beddard [21] have demonstrated that the comparison of steady-state anisotropy measurements between identical anthroyloxy probes in different lipid environments can also be complicated by molecular distortions that change the orientation of the emission transition moment. These complications are unresolved in steady-state anisotropy measurements and can only be distinguished by time-resolved studies.

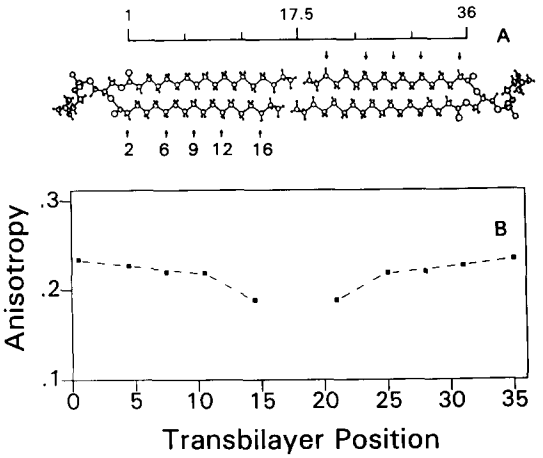

Fig. 5. The interdigitation signature of the C(18)C(18)PC gel-phase bilayer. Panel A is the molecular diagram of the noninterdigitated C(18)C(18)PC gel-phase bilayer which shows the positions (arrows) of the anthroyl moieties for probes located in both leaflets of the bilayer. Panel B is the corresponding transbilayer anisotropy profile derived by plotting the gel-phase anisotropy values of the PC probes (Fig. 4) against their transbilayer position. The scale used for determining the transbilayer positions of the anthroyl moieties is shown above the molecular diagram in panel A. Details are given in the text.

Thus, in the current study the anisotropy–position profiles of the mixed-acyl PC fluorescent probes are employed strictly as 'interdigitation signatures' (as discussed below) to identify the transbilayer organization of the host phospholipid bilayer. Although a hypothesis is presented to explain the fluorophore–lipid interactions responsible for the anisotropy–position profiles in the C(18)C(10)PC and C(10)C(18)PC bilayers, the relationship of these interactions to bilayer fluidity cannot be determined from the steady-state measurements reported here.

The mixed-acyl PC fluorescent probes were used to determine the anisotropy–position plots for the C(18)C(18)PC bilayers in the gel and liquid-crystalline phases. These plots are almost identical to those reported by Tilley et al. [11] and Thulborn et al. [22] for C(16)C(16)PC bilayers containing *n*-(9-anthroyloxy) fatty acids. As discussed previously, these plots are similar to the order parameter profiles obtained by NMR [12] and electron spin resonance [13] measurements of symmetric-chain PC bilayers. The gel-phase anisotropy–position plot shown in Fig. 4A represents the profile across one leaflet of the C(18)C(18)PC bilayer. A molecular diagram of the C(18)C(18)PC noninterdigitated gel-phase bilayer based upon X-ray diffraction results [18] is shown in Fig. 5A. This diagram reflects the conformational inequivalence of the two hydrocarbon chains that results in the *sn*-2 acyl chain being displaced 1.5 carbon–carbon bond lengths closer to the glycerol backbone relative to the fully extended *sn*-1 acyl chain [25]. The locations of the anthroyl moieties of the mixed-acyl PC probes in the bilayer are indicated in the diagram (by arrows) for probes in both bilayer leaflets. In assigning these locations, it is assumed that the anthroyloxy-labeled *sn*-2 acyl chains of the fluorescent probes lie at the same depth in the bilayer as the *sn*-2 stearoyl chains of the surrounding C(18)C(18)PC matrix. The accompanying transbilayer anisotropy profile for the C(18)C(18)PC gel-phase bilayer is shown in Fig. 5B. In this profile the anisotropies of the anthroyl moieties of the mixed-acyl

PC probes in both bilayer leaflets are plotted against their positions along the bilayer normal (transbilayer position). The numbering scheme for this axis is scaled to the positions of the carbons of the fully extended *sn*-1 acyl chain in the PC molecule on the left-hand side of the molecular diagram (Fig. 5A). The carbonyl carbon of this chain corresponds to position 1, the α-carbon to position 2, and so forth. A scale corresponding to this numbering scheme is shown above the molecular diagram. This profile reflects the low anisotropy at the bilayer center that arises from the disorder present at this location in the noninterdigitated bilayer and the intrinsically low anisotropy of the terminal anthroyl moiety [30].

The gel-phase anisotropy–position plots for the C(18)C(10)PC and C(10)C(18)PC bilayers cannot be compared directly to the corresponding plot for C(18)C(18)PC because the mixed-acyl PC probes penetrate past the midpoint of the mixed-interdigitated bilayer. Molecular diagrams of the C(18)C(10)PC and C(10)C(18)PC mixed-interdigitated gel phases are shown in Figs. 6A and 7A, respectively, in which the locations of the anthroyl moieties of the fluorescent probes penetrating from opposing sides of the bilayer are indicated. These diagrams are based upon X-ray diffraction analysis of these bilayers [1,18]. The corresponding transbilayer anisotropy profiles for the C(18)C(10)PC and C(10)C(18)PC gel-phase bilayers are shown in Figs. 6B and 7B, respectively. These transbilayer profiles were derived using the same procedures and assumptions that were described above for C(18)C(18)PC. These profiles reveal some interesting points. First, although they are located at different sites on the *sn*-2 acyl chain of the mixed acyl PC fluorescent probes, the anthroyl moieties of 9-AS-PC and 12-AS-PC are located at equivalent depths in the C(18)C(10)PC mixed-interdigitated bilayer. Accordingly, their anisotropy values are almost identical. Second, transbilayer anisotropy profiles of both mixed-acyl PC bilayers are characterized by maxima in the anisotropy values at the bilayer interface and in the vicinity of the terminal methyl pocket and by minima between these locations. Third, the transbilayer anisotropy profiles of the mixed-acyl PC bilayers are distinctly different from that of the noninterdigitated bilayer. Thus, the mixed-acyl PC fluorescent probes can be used to construct transbilayer anisotropy profiles that can serve as 'interdigitation signatures' for these two different gel-phase bilayer organizations.

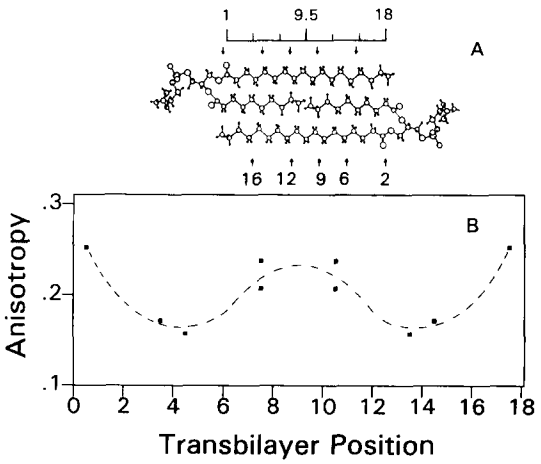

Fig. 6. The interdigitation signature of the C(18)C(10)PC gel-phase bilayer. Panel A is the molecular diagram of the mixed-interdigitated C(18)C(10)PC gel-phase bilayer showing the positions of the anthroyl moieties for probes located in both bilayer leaflets. Panel B is the corresponding transbilayer anisotropy profile. Other details are as given in Fig. 5.

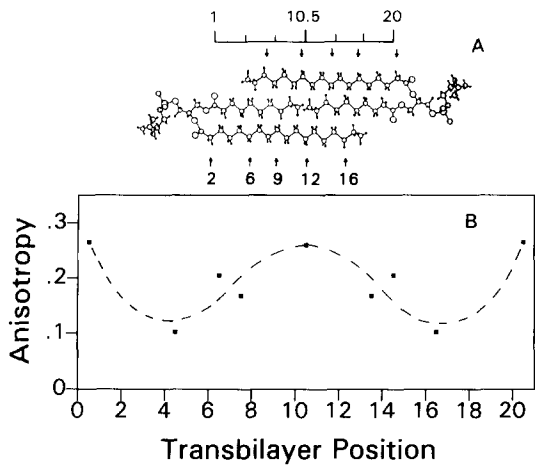

Fig. 7. The interdigitation signature of the C(10)C(18)PC gel-phase bilayer. Panel A is the molecular diagram of the mixed-interdigitated C(10)C(18)PC gel-phase bilayer showing the positions of the anthroyl moieties for probes located in both bilayer leaflets. Panel B is the corresponding transbilayer anisotropy profile. Other details are as given in Fig. 5.

Within the limitations discussed above, it is possible to present a tentative explanation for the shape of the transbilayer anisotropy profiles of the mixed-acyl PC bilayers. High relative anisotropy values for 2-(9-anthroyloxy) fatty acids, whose anthroyl moieties are located at the bilayer interface, are observed in most phospholipid bilayers [11,20,30]. Thus, the anisotropy maxima observed for the 2-AS-PC probe is not unexpected. High relative anisotropy values were also seen for probes whose anthroyl moieties are located in the vicinity of the terminal methyl pocket of the mixed-interdigitated bilayer. The acyl chains of the PC molecules will experience various limited dynamic motions in the bilayer gel phase. These include *trans* ↔ *gauche* isomerization [32] and chain reorientation and rotation about the bilayer normal [33]. The mixed-chain PCs also exhibit coupled whole-molecule rotator motions about their long molecular axes [34]. As a result of these motions, the caproyl chains from opposing

bilayer leaflets will not be in perfect register. This dynamic axial displacement may serve to restrict the rate of, or impose an orientational constraint on, the rotations (particularly the out-of-plane rotations) of the anthroyl moieties in the vicinity of the methyl pocket, thus rendering the relative anisotropy high in this region of the mixed-interdigitated bilayer.

The anisotropy minima in the transbilayer profiles are more difficult to interpret. One explanation is that the corresponding mixed-acyl PC probes are segregated into small regions of the bilayer due to probe clustering. The low relative anisotropy values could then arise from concentration-dependent depolarization of fluorescence [35]. A second explanation is that the steric interaction of the bulky anthroyl moieties with the surrounding acyl chains in this region of the bilayer leads to the formation of pockets in which the anthroyl moieties reside. The anthroyl moiety would be able to undergo relatively free out-of-plane rotation within these pockets, thus accounting for the low relative anisotropy values. A third explanation is that the anisotropy minima result from an increase in the fluorescence lifetime for the probes located in this region of the bilayer. Clearly, detailed time-resolved fluorescence studies will be required to distinguish among these possibilities.

Raman spectroscopic studies [26] have shown that the lipid acyl chains of all three PCs are highly disordered in the liquid-crystalline bilayer phase. Thus, it was unexpected to find that the anisotropy–position plots for the liquid-crystalline phase of the mixed-acyl PCs more closely resembled their respective gel-phase plots that the anisotropy–position plot for the C(18) C(18)PC liquid-crystalline phase. This suggests that the mixed-acyl PC bilayers do not expand to the point where a discrete bilayer center exists in the liquid-crystalline phase. As a result, the dynamic motions of the acyl chains in one bilayer leaflet are influenced, through excluded volume interactions, by the interpenetration of the disordered acyl chains from the opposing leaflet. Although no static interdigitation persists in the liquid-crystalline phase, a form of dynamic intermixing of the lipid acyl chains from opposing bilayer leaflets does appear to occur. This conclusion is in agreement with the X-ray diffraction results of McIntosh et al. [2], who concluded that C(18)C(10)PC packs in the liquid-crystalline phase with two chains per headgroup and a bilayer thickness that is consistent with significant overlap of the phospholipid acyl chains. It is probable that this effect is exacerbated for the mixed-acyl PC fluorescent probes due to the steric bulk of the anthroyl moieties.

In summary, the mixed-acyl PC fluorescent probes described here can be used to study the thermal behavior and transbilayer organization of symmetric-chain and mixed-acyl PC bilayers. The combination of DSC and fluorescence spectroscopy has led to the suggestion that, upon cooling, the C(18)C(10)PC liquid-crystalline phase converts to the mixed-interdigitated gel phase by way of a partially interdigitated gel-phase intermediate. Isothermal plots of anisotropy versus probe position can be used to construct transbilayer anisotropy profiles that serve as interdigitation signatures to distinguish the noninterdigitated from the mixed-interdigitated gel-phase packing. In this study the *n*-(9-anthroyloxy) fatty acids were covalently linked to a mixed-acyl PC host in order to be certain of their location in the bilayer. In future studies it will be determined if free *n*-(9-anthroyloxy) fatty acids can be also be used to construct transbilayer anisotropy profiles and if unique interdigitation signatures exist for other types of interdigitated bilayers such as the fully interdigitated bilayers characteristic of lysoPCs [25] and certain ether phospholipids [31].

References

[1] Hui, S.W., Mason, J.T. and Huang, C. (1984) Biochemistry 23, 5570–5577.
[2] McIntosh, T.J., Simon, S.A., Ellington, J.C. and Porter, N.A. (1984) Biochemistry 23, 4038–4044.
[3] Xu, H. and Huang, C. (1987) Biochemistry 26, 1036–1043.
[4] Mason, J.T. and Stephenson, F.A. (1990) Biochemistry 29, 590–598.
[5] Levin, I.W., Thompson, T.E., Barenholz, Y. and Huang, C. (1985) Biochemistry 24, 6282–6286.
[6] Boggs, J.M., Koshy, K.M. and Rangaraj, G. (1988) Biochim. Biophys. Acta 938, 373–385.
[7] Boggs, J.M., Rangaraj, G. and Watts, A. (1989) Biochim. Biophys. Acta 981, 243–253.
[8] Haigh, E.A., Thulborn, K.R. and Sawyer, W.H. (1979) Biochemistry 16, 3525–3532.
[9] Podo, F. and Blasie, J.K. (1977) Proc. Natl. Acad. Sci. USA 74, 1032–1036.
[10] Thulborn, K.R. and Sawyer, W.H. (1978) Biochim. Biophys. Acta 511, 125–140.
[11] Tilley, L., Thulborn, K.R. and Sawyer, W.H. (1979) J. Biol. Chem. 254, 2592–2594.
[12] Seelig, J. and Seelig, A. (1980) Quart. Rev. Biophys. 13, 19–61.
[13] Hubbell, W.L. and McConnell, H.M. (1971) J. Am. Chem. Soc. 93, 314–324.
[14] Vanderkooi, J., Fischkoff, S., Chance, B. and Cooper, R.A. (1974) Biochemistry 13, 1589–1595.
[15] Mason, J.T., Broccoli, A.V. and Huang, C. (1981) Anal. Biochem. 113, 96–101.
[16] Selinger, Z. and Lapidot, Y. (1966) J. Lipid Res. 7, 174–175.
[17] Gomori, G. (1942) J. Lab. Clinc. Med. 27, 955–960.
[18] Shah, J., Sripada, P.K. and Shipley, G.G. (1990) Biochemistry 29, 4254–4262.
[19] Boggs, J.M. and Mason, J.T. (1986) Biochim. Biophys. Acta 863, 231–242.
[20] Cadenhead, D.A., Kellner, B.M.J., Jacobson, K. and Papahadjopoulos, D. (1977) Biochemistry 16, 5386–5392.
[21] Thulborn, K.R. and Beddard, G.S. (1982) Biochim. Biophys. Acta 693, 246–252.
[22] Thulborn, K.R., Tilley, L.M., Sawyer, W.H. and Treloar, E. (1979) Biochim. Biophys. Acta 558, 166–178.

[23] Huang, N-n., Florine-Casteel, K., Feigenson, G.W. and Spink, C. (1988) Biochim. Biophys. Acta 939, 124–130.
[24] Florine, K.I. and Feigenson, G.W. (1987) Biochemistry 26, 1757–1768.
[25] Huang, C. and Mason, J.T. (1986) Biochim. Biophys. Acta 684, 423–470.
[26] Huang, C., Mason, J.T. and Levin, I.W. (1983) Biochemistry 22, 2775–2780.
[27] Mason, J.T., Huang, C. and Biltonen, R.L. (1983) Biochemistry 22, 1013–1018.
[28] Kawato, S., Kinosita, K. and Ikegami, A. (1977) Biochemistry 16, 2319–2324.
[29] Vincent, M., De Foresta, B., Gallay, J. and Alfsen, A. (1982) Biochemistry 21, 708–716.
[30] Matayoshi, E.D. and Kleinfeld, A.M. (1981) Biophys. J. 35, 215–235.
[31] Ruocco, M.J., Siminovitch, D.J. and Griffin, R.G. (1985) Biochemistry 24, 2406–2411.
[32] Yellin, N. and Levin, I.W. (1977) Biochim. Biophys. Acta 489, 177–190.
[33] Lange, A., Marsh, D., Wassmer, K.-H., Meier, P. and Kothe, G. (1985) Biochemistry 24, 4383–4392.
[34] Xu, H., Stephenson, F.A. and Huang, C. (1987) Biochemistry 26, 5448–5453.
[35] Bashford, C.L., Morgan, C.G. and Radda, G.K. (1976) Biochim. Biophys. Acta 426, 157–172.